

## A Review of Passive Power Filters for Three-Phase Grid-Connected Voltage-Source Converters

Beres, Remus Narcis; Wang, Xiongfei; Liserre, Marco; Blaabjerg, Frede; Bak, Claus Leth

*Published in:*

I E E E Journal of Emerging and Selected Topics in Power Electronics

*DOI (link to publication from Publisher):*

[10.1109/JESTPE.2015.2507203](https://doi.org/10.1109/JESTPE.2015.2507203)

*Publication date:*

2016

*Document Version*

Accepted author manuscript, peer reviewed version

[Link to publication from Aalborg University](#)

*Citation for published version (APA):*

Beres, R. N., Wang, X., Liserre, M., Blaabjerg, F., & Bak, C. L. (2016). A Review of Passive Power Filters for Three-Phase Grid-Connected Voltage-Source Converters. *I E E E Journal of Emerging and Selected Topics in Power Electronics*, 4(1), 54-69. <https://doi.org/10.1109/JESTPE.2015.2507203>

### General rights

Copyright and moral rights for the publications made accessible in the public portal are retained by the authors and/or other copyright owners and it is a condition of accessing publications that users recognise and abide by the legal requirements associated with these rights.

- Users may download and print one copy of any publication from the public portal for the purpose of private study or research.
- You may not further distribute the material or use it for any profit-making activity or commercial gain
- You may freely distribute the URL identifying the publication in the public portal -

### Take down policy

If you believe that this document breaches copyright please contact us at [vbn@aub.aau.dk](mailto:vbn@aub.aau.dk) providing details, and we will remove access to the work immediately and investigate your claim.



# A Review of Passive Power Filters for Three-Phase Grid-Connected Voltage-Source Converters

Remus Narcis Beres, *Student Member, IEEE*, Xiongfei Wang, *Member, IEEE*, Marco Liserre, *Fellow, IEEE*, Frede Blaabjerg, *Fellow, IEEE*, and Claus Leth Bak, *Senior Member, IEEE*

**Abstract**—In order to reduce size and cost, high-order passive filters are generally preferred in power converters to cancel out high-frequency harmonics caused by pulswidth modulation. However, the filter resonance peaks may require the use of passive dampers to stabilize the interactions between the load and source impedances. Furthermore, the stabilizing effect is more difficult to be guaranteed for cost-optimized filters, which are characterized by low-inductance and high-capacitance passive components. In this paper, several passive filter topologies used to interface voltage-source converters with the utility grid are reviewed and evaluated in terms of damping capability, stored energy in the passive components, and power loss in the damping circuit. In addition, the influences of different switching frequencies of power converters on the passive filter design are discussed in the range 1–15 kHz. Illustrative design examples of the passive filters and experimental data are also provided.

**Index Terms**—LCL filter, passive filters, resonance damping, trap filter, voltage-source converters (VSCs).

## I. INTRODUCTION

DESIGNING passive filters is known to be a complex task [1]. When the harmonic source is a grid-connected voltage-source converter (VSC), then different harmonic spectra on the converter side of the passive filter [2], possible resonance conditions (due to the interaction of the filter with the system impedance) [3], or variation of the harmonic emission with the operating point of the power converter are just a few prerequisites that have to be considered in the design procedure of the passive filter [4]. The harmonic content in a steady-state operation at the point of common coupling (PCC) is, in general, limited by grid connection standards. Several harmonic limits for low-voltage (LV) networks (e.g., VDE-AR-N 4105 [5]), medium-voltage (MV) networks (e.g., BDEW [6]), and LV/MV networks (e.g., IEEE 1547 [7]) are summarized in Table I.

At the component level, additional design considerations are related to the physical design of the passive filter,

Manuscript received May 29, 2015; revised September 1, 2015 and November 12, 2015; accepted December 6, 2015. This work was supported by the European Research Council (ERC) through the European Union's Seventh Framework Program (FP/2007-2013)/ERC under Grant 321149-Harmony. Recommended for publication by Associate Editor T.-J. Liang.

R. N. Beres, X. Wang, F. Blaabjerg, and C. L. Bak are with the Department of Energy and Technology, Aalborg University, Aalborg 9220, Denmark (e-mail: rnb@et.aau.dk; xwa@et.aau.dk; fbl@et.aau.dk; clb@et.aau.dk).

M. Liserre is with the Department of Power Electronics, University of Kiel, Kiel D-24143, Germany (e-mail: ml@tf.uni-kiel.de).

Color versions of one or more of the figures in this paper are available online at <http://ieeexplore.ieee.org>.

Digital Object Identifier 10.1109/JESTPE.2015.2507203

TABLE I

HARMONIC CURRENT LIMITS (% OF RATED CURRENT)  
FOR SEVERAL GRID CONNECTION STANDARDS

Harmonic order, $h$	VDE-AR-N 4105 (LV) [5]	BDEW (MV)* [6]	IEEE 1547 (LV & MV) [7]
5	2.08	2.06	4
7	1.39	2.84	4
11	0.69	1.8	2
13	0.55	1.32	2
17	0.42	0.76	1.5
19	0.35	0.62	1.5
23	0.28	0.42	0.6
25	0.21	0.35	(23 ≤ h < 35)
25 < h < 40	5.2/h	8.67/h	0.3
40 < h < 180	6.24/h	6.24/h	(h > 35)

\*referred to 400 V and a Short Circuit Ratio (SCR) of 20.

such as the following:

- 1) magnetic material adopted for the filter inductors [8], [9];
- 2) loss and temperature rise in the inductors [10];
- 3) cooling method [10], [11].

To account for all the aforementioned design factors, multiobjective optimization of the overall conversion system is to be considered, and all can influence on the cost, size, and efficiency of the filter [12]. In addition, the filter design also depends on the adopted filter topology. For a simple inductor ( $L$  filter), which is illustrated in Fig. 1, together with other typical passive filter configurations, the resonance of the filter with the system impedance is avoided, since the utility grid is inductive below a few kilohertz in most applications. A large inductance in the  $L$  filter is required to limit the high-frequency switching ripple, which results in a bulky and expensive passive filter. However, the low ripple condition leads to a very high efficiency, similar to 50/60 Hz utility transformers. The drawbacks are very high cost and excessive voltage drop across the inductor, which limits the use of this solution for applications above several kilowatts [13], unless interleaved [14] or multilevel VSCs [15] are employed. On the other hand, a low-pass  $LC$  or  $LCL$  filter provides two or three times more attenuation depending on the adopted cutoff frequency. As a result, a reduced size and cost of the filter

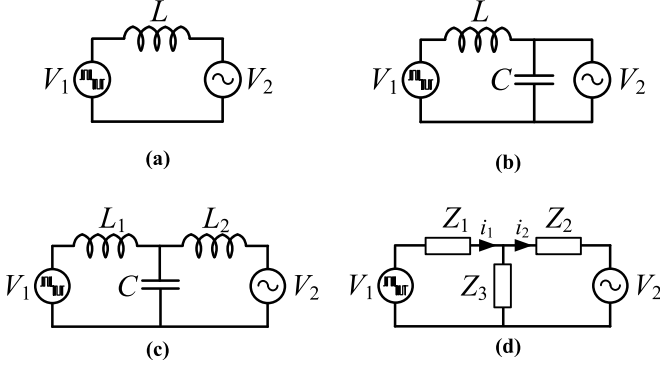


Fig. 1. Passive filters for a two-level grid-connected VSC (per-phase schematics with  $V_1$  the line to line converter voltage and  $V_2$  is the PCC voltage). (a)  $L$  filter. (b) Low-pass  $LC$  filter. (c) Low-pass  $LCL$  filter. (d) Generalized high-order filter model.

can be obtained. On the assumption that the grid impedance is inductive, the  $LC$  filter can be perceived as an  $LCL$  filter. More complex passive filters, including single or multiple shunt-connected  $LC$ -traps [16], can be simplified in a similar way to the  $LCL$  filter, by using the generalized high-order filter model from Fig. 1(d).

Particular contributions related to the  $LCL$  filter design may include the following:

- 1) parameter selection based on a conceptual approach [13];
- 2) parameter selection based on detailed analytical model of the filter [17];
- 3) optimization based on parameter selection and physical design of the passive components [12].

The  $LCL$  filter [18] can be seen, to some extent, as a generalized interfaced high-order filter model (T equivalent circuit), which can describe the stability interactions between the load and source impedance of grid-connected VSCs [19], [20]. The resonance peaks inherent to high-order passive filters may require the use of damping to stabilize the interactions between the load and the source impedances. Explicitly, the filter resonances increase the risk of harmonic amplification at the PCC and can deliberately be avoided by the use of shunt passive-damped filters [21] or active damping control methods [22]. However, in the case of cost-optimized filters, characterized by low-inductance and high-capacitance passive components [23]–[25], the resonance damping is more difficult to be guaranteed. High capacitance in the filter results in high ripple content, both at the converter side inductance and capacitor current/voltage, which adds cost to the sensing system needed to measure the feedback variables required for active damping methods. Sensorless active damping can also be employed, by cascading a digital filter with the current controller loop; however, they are sensitive to parameter variations and system uncertainties [26]. On the other hand, the use of passive damping methods increase the VAr rating of the filter and the associated damping losses [27] in such a way that passive damping is not practical to implement [28]. Then, there is limited evidence of how significant the passive damping losses are, especially for high harmonic current in the shunt capacitor of the filter. To stabilize the control system,

proper passive-damped filter solutions and their evaluation for a wide range of operating scenarios become interesting from a practical design point of view (e.g., to minimize the damping losses).

Several passive filter topologies to dampen the filter resonance have been reviewed or discussed in [29]–[31]. However, only limited information about the choice of the damping circuit ratings is given. In [32] and [33], a comparative analysis of the filters is completed for a fixed switching frequency, and one cannot decide which filter topology is best suited, if the application or target switching frequency of the VSC is different [34]. In addition, the amount of resonance damping attenuation and its impact on the dynamic performance of the current controllers and system stability are omitted. Therefore, in this paper, several passive filter topologies used to interface the VSCs with the utility grid are reviewed and evaluated in terms of damping capability, stored energy in the passive components, and power loss in the damping circuit. The damping capability is evaluated using the optimal passive damping design method proposed in [35], while the maximum peak criteria applied in [36] are adopted to ensure the stability of the control system. In addition, the influences of different operating switching frequencies of power converters on the passive filter design are also discussed in the range 1–15 kHz.

An overview of the  $LCL$  filter design procedures is described in the forthcoming section with design examples for illustration. In Section III, the selection of several passive filter topologies for dampening the filter resonances is presented. In Section IV, a discussion on the applied methods used to evaluate the passive filters is given. Then, the evaluation of the passive filters is performed for different operating conditions, including different switching frequencies, attenuation requirements, and position of the current sensors. Experimental validation and conclusions complete the content of this paper.

## II. OVERVIEW OF $LCL$ FILTER DESIGN

The design of high-order filters is consistent with the  $LCL$  filter design in most situations [37]. Therefore, different design criteria are given for the  $LCL$  filter in the following.

### A. Conventional $LCL$ Filter Design

A step-by-step design procedure for an  $LCL$  filter was introduced in [13]. It was suggested that the resonance frequency of the filter should lie between ten times the line frequency and half the switching frequency in order to ensure effective attenuation of the switching harmonics, and to prevent resonances caused by switching harmonics or low-order harmonics from grid background voltage distortion. The design guidelines apply for an operating switching frequency ( $f_s$ ) of 5~10 kHz [37]–[43]. In addition, the design procedure proposed in [13] enables a relatively fast design of the passive filter with a reduced number of iterations [25]. For example, it can be summarized as the following.

- 1) Select the converter side inductance ( $L_1$ ) based on desired maximum current ripple in inductor ( $\Delta i_{1\max}$ ). A rough estimation of the maximum current ripple in the inductor for a three-phase VSC with the conventional space vector modulation (SVM) can be found from the

volt-second balance principle across the inductor during one instance of the switching period ( $1/f_s$ ) [44]

$$L_1 = \frac{V_{dc}}{24f_s \Delta i_{1\max}} \quad (1)$$

where  $V_{dc}$  is the dc-link voltage of the VSC.

- 2) Select filter capacitance ( $C$ ) as a percentage ( $x$ ) of the base capacitance at rated conditions

$$C = x\% \frac{S}{2\pi f_1 V_{ll}^2} \quad (2)$$

where  $S$  is the apparent power of the VSC,  $f_1$  is the fundamental frequency of the grid, and  $V_{ll}$  is the grid line to line voltage. The capacitor value should be limited to 5% in order to not decrease the power factor.

- 3) The total inductance should be limited to 10% in order to limit the voltage drop across the inductors.

Additional dependencies between the filter capacitance and voltage drop across the filter inductors and ac sensors position (used for the reference current control and grid synchronization) were introduced in [45] in order to not overrate the VSC. In [46], the total inductance of the *LCL* filter is adopted based on a desired control bandwidth that should ensure the VSC controllability. In [38], a split function is used to divide the total inductance of the filter between the converter and grid side inductance. It was shown that in order to limit the current ripple in the converter side inductance (to reduce power loss in the filter) and increase the filter attenuation, it is required that the converter side inductance be dominant in the filter. The filter design based on the consideration of the converter current ripple and some attenuation requirements was proposed in [47]. A similar work is presented in [48] with useful analytical expressions given on how to design the converter side inductor with respect to the saturation level of the magnetic core. The drawback of the above design methods is the conservative choice of parameters, especially for an inexperienced practicing engineer.

### B. Optimal Design With Minimization of the Stored Energy

The optimization of the filter parameters based on the minimum stored energy with additional considerations on the ripple current, dc-link voltage reserve for controllability, and attenuation of the filter (derived based on specified harmonic standard limits and analytical solutions of the harmonic voltage spectrum related to the pulse width modulation (PWM) method) are given in [17]. Referring to the notations given in Fig. 1(d), an optimal design method of the *LCL* filter can be performed as follows.

- 1) *Define the State-Space Model of the Filter*: The currents on the converter ( $i_1$ ) and grid side ( $i_2$ ) of the filter can be written as function of the converter voltage ( $V_1$ ), grid voltage ( $V_2$ ) and the corresponding filter admittances, as [32]

$$\begin{bmatrix} i_1 \\ i_2 \end{bmatrix} = - \begin{bmatrix} Y_{11} \\ Y_{22} \end{bmatrix} V_1 - \begin{bmatrix} Y_{12} \\ Y_{22} \end{bmatrix} V_2. \quad (3)$$

The filter input admittance ( $Y_{11}$ ), filter reverse transadmittance ( $Y_{12}$ ), filter attenuation or forward transadmittance ( $Y_{21}$ ) and filter output admittance ( $Y_{22}$ ) in (3) can be written as a function of the equivalent impedances of the filter components [32]

$$\begin{bmatrix} Y_{11} \\ Y_{12} \\ Y_{21} \\ Y_{22} \end{bmatrix} = \frac{1}{Z_1 Z_2 + Z_1 Z_3 + Z_2 Z_3} \begin{bmatrix} Z_2 + Z_3 \\ -Z_3 \\ Z_3 \\ Z_1 + Z_3 \end{bmatrix}. \quad (4)$$

- 2) Calculate the amplitude of the converter voltage harmonics,  $V_1(h)$ , according to the selected PWM method using a simulation platform. To reduce the computational time [25], the amplitude of the individual voltage harmonics can be analytically calculated as indicated in [2] as a function of the harmonic order, dc-link voltage, and modulation index.
- 3) Calculate the maximum filter admittance ( $Y_{21\max}$ ) required to ensure the attenuation of dominant harmonics specific to the PWM method according to applicable harmonic current limits ( $i_{\text{limit}}$ ) defined in grid connection standards or other power quality standards, for example, one of those indicated in Table I

$$Y_{21\max}(h) = \frac{i_{\text{limit}}(h)}{V_1(h)}. \quad (5)$$

- 4) Choose the filter components based on the allowable current ripple in the converter side inductance, overrating of the VSC, and so on, by fulfilling the following filter admittance attenuation condition:

$$Y_{21}(h) \leq Y_{21\max}(h). \quad (6)$$

In Fig. 2(a), the attenuation admittance  $Y_{21}(h)$  is evaluated for a switching/sampling frequency ( $f_s$ ) of 10 kHz at the  $(m_f - 2)$  harmonic order as a function of the variation of reasonable values of the *LCL* filter parameters (where  $m_f$  is the modulation frequency, defined as the ratio between the switching frequency and the fundamental frequency). Assuming that the SVM method is used,  $Y_{21\max}(m_f - 2)$  is -60 dB for the IEEE 1574 standard. The characteristic frequency of the filter ( $f_0$ ), defined as the resonance frequency of the filter when there is no resistance in the passive filter, is shown in Fig. 2(b).

Fig. 2 shows that for a 10-kHz VSC, resonance frequencies lower than  $\sim 0.2 f_s$  will lead to conservative designs of the passive filter. From Fig. 2(a), there are sufficient solutions in the design space that fulfills the admittance attenuation condition. To reduce the size and cost of the passive filter, some additional design constraints can be imposed, such as the limitation of stored energy in the inductive components [17], [23]–[25]. In [17], it has been shown that different sets of filter parameters can cause the same attenuation of the filter or similar transient response. Similar conclusions were obtained in [23], when the optimization was performed for different weight ratios between the stored energy of the inductors and capacitors.

The contributions from the filter and the grid equivalent resistances are taken into account in [24], where the filter

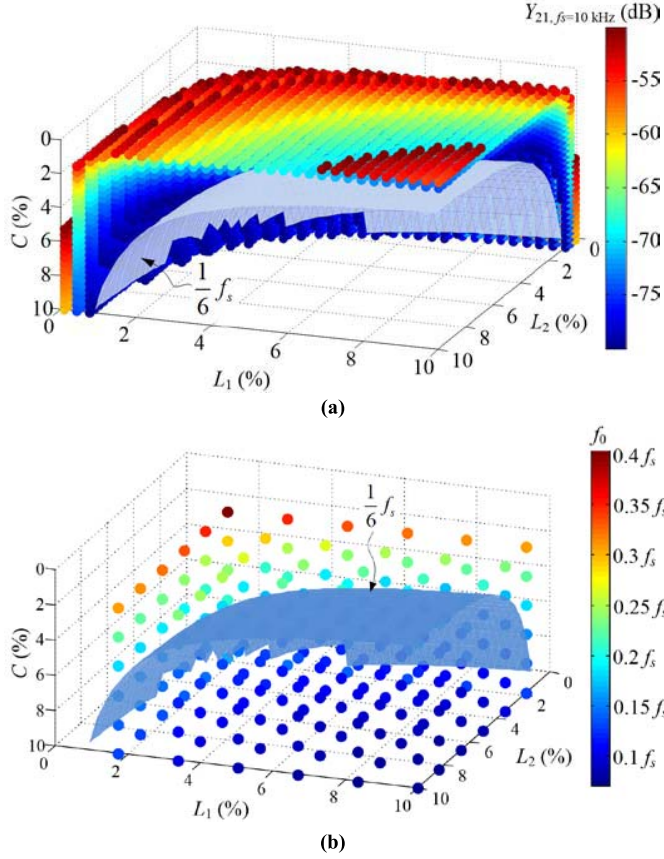
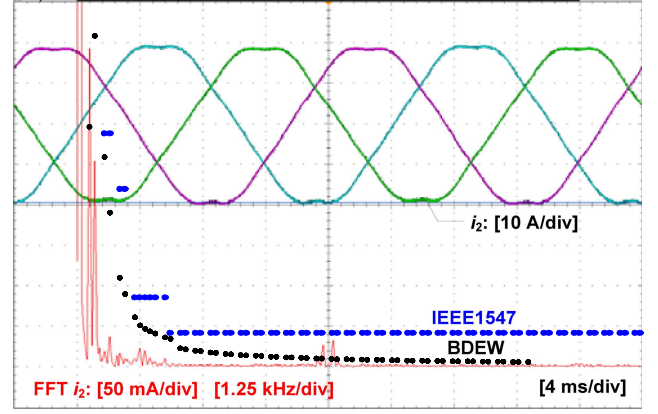


Fig. 2.  $LCL$  filter parameters variation as function of (a) high-frequency attenuation admittance,  $Y_{21}$  ( $f_s = 10$  kHz) and (b) characteristic frequency,  $f_0$ .

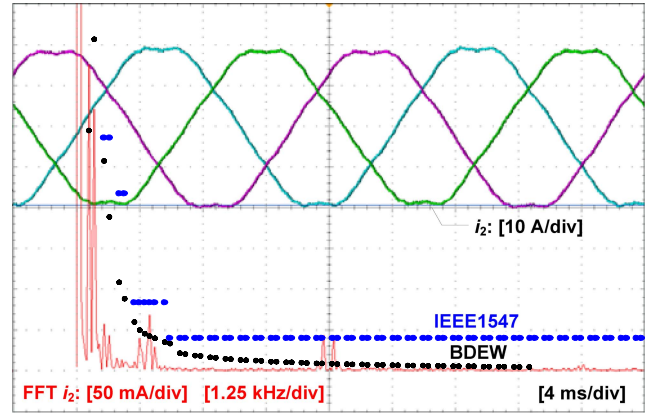
is optimized in order to obtain minimum-cost inductors (and therefore filter), which results in very low percentage inductors and high capacitance values. In [25], the total inductance of the filter is minimized for a variable grid frequency specific to aircraft power systems, with relatively high values of the filter capacitors (suggested for the synchronous SVM). However, a high capacitance value in the filter decreases the resonance frequencies in the filter, which, in turn, increases the low-frequency harmonic content and the total harmonic distortion (THD) of the grid current [23]. As a consequence, the optimization of filter parameters, which takes into account the THD limits, is suggested in [49] by considering both the open and closed loop forms of the filter and control system. In [50], the minimization of the total inductance of the filter, which leads to a minimum rms current in the converter side inductance is obtained for an  $LCL$  filter applied to a MW range VSC. As a result, a very high filter percentage capacitance ( $\sim 40\%$ ) was obtained.

### C. $LCL$ Filter Design Comparison Between Conventional and Optimal Approach

A two-level 10-kW VSC with a 5-kHz switching frequency is selected to review the previous two design methods. Assuming about 10% ripple in  $L_1$ , the resulting inductance is 3.5 mH or 7% according to (1). A 5% filter capacitance from (2) translates into 9.5  $\mu\text{F}$  capacitance. The grid side inductance  $L_2$  is selected 3% or 1.5 mH according



(a)  $L_1=3.5\text{mH}$  (7%),  $L_2=1.5\text{mH}$  (3%),  $C=9.5\mu\text{F}$  (5%),  $R_d=1.4\Omega$  (0.13%),  $P_d=0.03\%$ ,  $K_p=8.5$ ,  $K=450$



(b)  $L_1=2\text{mH}$  (4%),  $L_2=1.5\text{mH}$  (3%),  $C=20\mu\text{F}$  (10%),  $R_d=1.6\Omega$  (0.3%),  $P_d=0.4\%$ ,  $K_p=5$ ,  $K=250$

Fig. 3. Measurements for a designed  $LCL$  filter showing the output current harmonics response compared with IEEE 1547 and BDEW limits for a 10-kVA VSC with converter current control and  $V_{dc} = 700$  V and  $f_s = 5$  kHz. (a) Conservative approach. (b) Optimized filter.

to condition 3) from Section II-A. The optimal design method considers the minimization of the stored energy in the filter inductors (7% total inductance and 10% capacitance are chosen). The steady-state current waveform and the filter/VSC ratings are shown in Fig. 3(a) for the conservative approach and in Fig. 3(b) for the optimized filter. The size of the filter for the optimized scenario results in decreased size/cost of the filter by roughly 35%. However, the power losses in the damping resistor used to avoid oscillations are increased by a factor of 13 due to the increased capacitance and increased ripple in the filter inductance. Consequently, the low-order harmonics are more severe (measurements made under same grid condition).

The above example is only to illustrate some possible design scenarios. For the elevated switching frequency, the conservative approach will lead to an increased size compared with the given example. The design of the filters fulfills the IEEE 1547 standard. The more stringent BDEW recommendations imply the use of increased ratings to fulfill the grid connection requirement.

TABLE II  
POWER LOSS IN THE VSC AND *LCL* FILTER  
WITH LAMINATED Fe-Si INDUCTORS(%)

Reference	Frequency range	VSC loss	Filter loss	Core loss calculation method	Verified
[51]	2~6 kHz	0.8~1.5 %	0.1~0.2 %	iGSE	–
[53]	2~12 kHz	0.5~1 %	0.3~0.5 %	NSE	–
[12]	3~12 kHz	0.5~1.2 %	1.2~2.2 %	i <sup>2</sup> GSE + loss mapping	yes

#### D. Parameter Selection Based on Physical Design of Passive Components

All aforementioned designs neglect the influence of the high ripple content and the associated losses in the converter side inductance current due to minimized inductance. Especially, there is an efficiency versus size/cost tradeoff, which dictates the final choice of parameters. In [51], the improved generalized Steinmetz equation (iGSE) is used to investigate the loss of the filter with the aim to minimize the weight of a 2~6 kHz power filter used in a 1.2-MVA VSC. The Pareto front optimization of the power loss of inductors and semiconductors reveal only a small range variation of the inductor and semiconductor losses (20–30%) with changing the modulation method, core material (laminated Fe-Si versus amorphous), or winding material (Cu versus Al).

The weight of the filter can be decreased by a factor of 4 by increasing the total VSC losses with 50%. Power loss of inductors are in the range 0.1~0.2% while the semiconductor losses are in the range 0.8~1.5% depending on the aforementioned variables. The presence of a 5% grid inductance can reduce the filter weight by roughly 40%. However, these results are open for interpretation, since the iGSE method cannot accurately describe the inductor core loss under PWM excitation and dc-bias field strength [52].

In [53], the power loss in the *LCL* filter and VSC are evaluated at no-load condition using the natural Steinmetz extension method. Here, the core loss results in the range of 0.3%~0.5% for a switching frequency of 2~12 kHz, while the power loss in the semiconductors as 0.5%~1% depending on the modulation method and dc-link voltage. However, the evaluation of instantaneous iron loss in the inductors in [54] show that under load conditions the core loss can be significantly higher. Therefore, different optimized designs of the *LCL* filter are performed for the grain-oriented Fe-Si material in [12] using more accurate loss models. It is shown that adopting around 20% maximum ripple in the converter side inductance, the total filter loss is in the range of 1.2~2.2% depending on the adopted volume and switching frequency of the filter. The *LCL* filter prototype built in [12] yields around 1.8% total power loss, out of which ~80% of the loss is related to the converter side inductance only. In Table II, a summary of power losses in the VSC (semiconductor and switching loss) and losses in the passive filter is made.

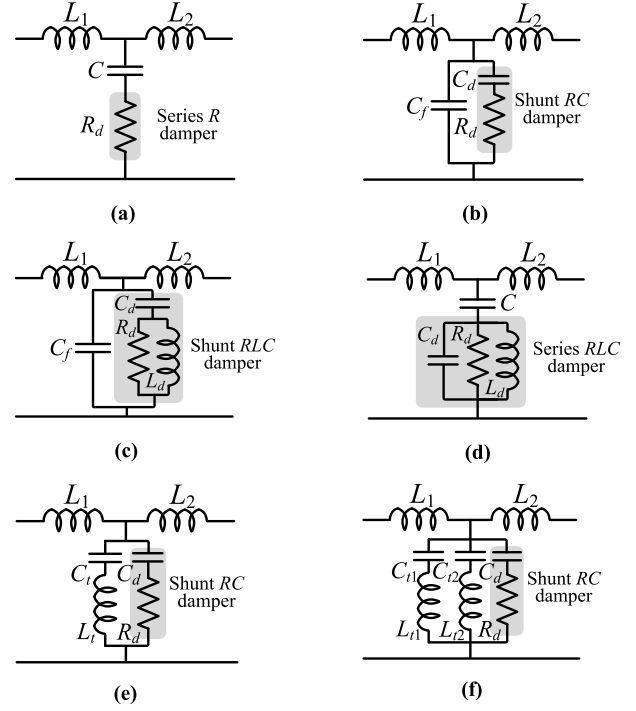


Fig. 4. Selected passive-damped filters to be used in grid-connected VSCs (damper name is referred to with respect to the filter capacitor position). (a) *LCL* filter + series damper. (b) *LCL* filter + shunt  $RC$  damper. (c) *LCL* filter + shunt  $RLC$  damper. (d) *LCL* filter + series  $RLC$  damper. (e) Trap + shunt  $RC$  damper. (f) 2traps + shunt  $RC$  damper.

### III. FILTER TOPOLOGY SELECTION

It was previously mentioned how a low-pass *LCL* filter [18] or a trap filter [40] adopted to cancel the ripple content related to the switching device operation can benefit from reduced size and cost. Both filter configurations originate from traditional passive filters used in power system transmission or HVDC systems [27]. The choice of the passive damping topology used to limit the resonance condition of the filters is, in general, based on the conventional shunt passive-damped filters specific to power systems [1], [27], [55] or may be based on shunt or series passive damping methods found in traditional low power dc-dc converter applications [56], [57]. When no physical passive damping circuit is adopted, the equivalent circuit of the filter should consider some damping in order to account for the frequency dependence or the parasitic effects of the passive components. From the passive filter topologies presented in [1], [27], and [55]–[57] only a few are found practicable in today's power conversion units.

#### A. *LCL* Filter With Series Resistor

A damping resistor in series with the filter capacitor is one of the most adopted passive damping solutions due to its simplicity in design and implementation [13]. This filter solution is illustrated in Fig. 4(a) with the equivalent series resistance of inductors omitted for simplicity. The damping resistor can also be placed in parallel with the filter capacitor but this solution is not practical since a high ripple current will flow into the resistor [30]. The attenuation performance of the filter can be analyzed by the filter attenuation admittance  $Y_{21}$  given in (4). Calculating for the *LCL* filter with damping

resistor, it results in

$$Y_{21}(s) = A_0 \frac{\frac{Q}{\omega_0} s + 1}{\frac{s^2}{\omega_0^2} + \frac{Q}{\omega_0} s + 1} = A_\infty \frac{\frac{\omega_0}{Q} \cdot s + 1}{\frac{\omega_0^2}{s^2} + \frac{\omega_0 Q}{s} + 1} \quad (7)$$

where  $A_0$  denotes the filter characteristic at frequencies lower than the characteristic frequency  $\omega_0$ ,  $A_\infty$  is the characteristic above  $\omega_0$  and  $Q$  the quality factor of the overall filter [44].  $A_0$ ,  $A_\infty$ ,  $\omega_0$  and  $Q$  can be written as

$$A_0 = \frac{1}{s(L_1 + L_2)} \quad A_\infty = \frac{R_d}{L_1 L_2 s^2} \\ Q = R_d \sqrt{\frac{C_\Sigma}{L_\Sigma}} = \frac{R_d}{R_0} \quad \omega_0 = \sqrt{\frac{1}{L_\Sigma C_\Sigma}} \quad (8)$$

where  $L_\Sigma$  is the equivalent inductance given by the parallel connection of  $L_1$  and  $L_2$ ;  $C_\Sigma$  is the equivalent capacitance of the filter given by  $C$ ;  $R_d$  is the damping resistor and  $R_0$  is the characteristic resistance of the filter. For shunt passive damping methods,  $A_0$  have the same formulation as indicated in (8). However, the high-frequency attenuation asymptote given by  $A_\infty$  will change depending on the adopted passive filter.

#### B. LCL Filter With Shunt RC Damper

An improved damping solution can be the shunt *RC* damper illustrated in Fig. 4(b). The main benefit of this filter is that the high-frequency attenuation of the filter is retained to 60-dB/decade. In addition, the power losses in resistor can decrease with a proper choice of the split capacitor ratio [58]. More details about this filter topology can be found in [35].

#### C. LCL Filter With Shunt RLC Damper

A good high-frequency attenuation and very low damping loss can be obtained by the second-order damped filter (*RLC* circuit in parallel with the filter capacitor) as illustrated in Fig. 4(c) [29], since the fundamental current in the resistor is bypassed by the additional damping inductance  $L_d$ .

#### D. LCL Filter With Series RLC Damper

Similar benefits can be obtained by the use of a selective resonant circuit as proposed in [32] and illustrated in Fig. 4(d). The filter contains an additional parallel *RLC* circuit connected in series with the filter capacitor in which the damping inductor and the capacitor selectively bypasses the damping resistor at low and high frequencies.

The damping element can also be placed in parallel or in series with the grid side inductor [44]. However, the maximum resonance attenuation that can be obtained is more limited compared with the previous damping solutions. In addition, the hardware implementation is impractical, especially if there is no physical grid side inductor in the filter.

#### E. Trap Filter With Shunt RC Damper

The close-to-zero impedance of the trap filter around the switching harmonics makes it possible to decrease the size of the filter even more compared with the *LCL* filter [4], [37], [59]–[62]. However, above the tuning frequency,

the trap filter is purely inductive and the overall filter attenuation is reduced to only 20 dB/decade. Therefore, an additional capacitor connected in parallel with the trap filter can increase the high-frequency attenuation [60], [61]. However, the presence of multisplit capacitors in the trap filter creates multiple resonances in the filter [61], [62], which increases the risk of resonance amplification between the grid and the filter. Theoretically, the same damping methods can be used for the trap filter as in the *LCL* filter case. However, the passive damping is more difficult for the trap filter, since the filter components count increases and the advantages over the *LCL* filter are reduced [33].

A shunt *RC* damping circuit seems to be a natural choice to damp the trap filter resonance as presented in [60], [62], and [63]. Such circuit is presented in Fig. 4(e).

#### F. 2traps Filter With Shunt RC Damper

The reduction of the filter size is further possible by adopting multiple single tuned filters in the *LCL* filter configuration [16] (filter volume decreased by  $\sim 50\%$  in [35] using two single tuned filters). In [64], it was shown that is possible to decrease the filter volume by adopting up to three traps tuned at the switching frequency and its multiples. The shunt *RC* damper used for the *2traps* filter is illustrated in Fig. 4(f). Similar to the *LCL* filter, the design procedures for the trap filters were proposed in [4], [35], [37], [40], [60], [64], and [65].

### IV. PASSIVE DAMPING DESIGN AND STABILITY CRITERIA

A decreased size and cost of the filter implies to minimize the filter inductance by adopting a higher current ripple in the converter side inductance and a consequently larger capacitance to ensure the same attenuation performance. To retain reasonable power loss in the filter (less than 2%) implies adopting magnetic materials, which can ensure low losses under the high ripple condition [66]. This inevitably leads to an increased risk of harmonic instabilities as results in low resonance frequencies due to high filter capacitance and/or high ripple in the converter side current. To stabilize the interactions between the source and load impedances, the power losses caused by the use of passive damping circuits should be very limited in order not to reduce the system efficiency significantly [67].

#### A. Passive Damping Design

While a large set of solutions are available for the practicing engineer when an *LCL* or a trap filter is chosen (as indicated in the design space from Fig. 2), the design of the passive damping circuit is typically straightforward. For instance, if only a series resistor as shown in Fig. 4(a) is adopted, then its value can be found from (8) as percentage ( $y$ ) of  $R_0$

$$R_d = y\% R_0. \quad (9)$$

The parameter  $y$  should be limited up to 30% (resulting in a maximum quality factor of 0.3) in order to limit the power loss in the resistor and to ensure enough attenuation of the filter resonant peaks. For more complex passive filters

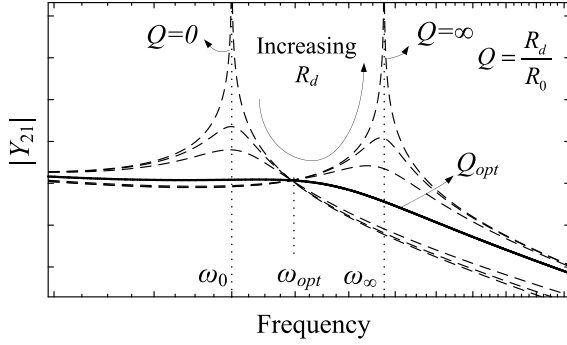


Fig. 5. Optimum quality factor and frequency for passive filters with split capacitors and/or inductors.

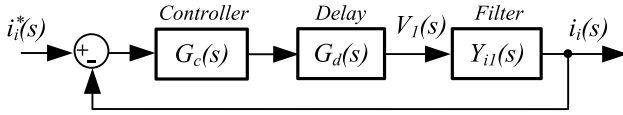


Fig. 6. Current control structure of an VSC connected to an ideal grid voltage source ( $i = 1$ : converter current is controlled,  $i = 2$ : grid current is controlled).

with split capacitors or inductors, the design methods given in [35] and [56] can be used to derive the value of the damping resistor. It can be briefly summarized as follows.

- 1) Design the main passive filter parameters without additional damping, using either of the design method given in Section II and calculate the filter characteristic resistance  $R_0$  and frequency,  $\omega_0$  using (8).
- 2) Find the optimum frequency ( $\omega_{opt}$ ) and quality factor ( $Q_{opt}$ ) of the filter with damping circuit which minimizes the peak in the filter attenuation admittance. Analytical solutions are given in [35] for the passive filters illustrated in Fig. 4(b), (e), and (f). For other passive filter topologies, the optimum damping parameters can be found using similar derivations. In Fig. 5, the principle of optimum damping is illustrated for passive-damped filters with split capacitor and/or inductors.
- 3) Choose the ratio of the split capacitors and/or inductors and decide the final value of the quality factor as a tradeoff between damping performance (attenuation of the resonance peak) and power loss in the damping resistor.

### B. Stability Criteria and Transient Performance

The closed loop current controller for the converter ( $i = 1$ ) or grid side current ( $i = 2$ ) feedback is illustrated in Fig. 6. The closed loop system includes the current controller ( $G_c$ ), the delay due to digital computation ( $G_d$ ) and the plant of the control loop given by the filter ( $Y_{ii}$ ). The delay is responsible for a phase lag in the control system and typically accounts for up to about 1.5 of the sampling period  $T_s$  [45]. The Nyquist stability criterion can be used to assess the control stability, i.e., no  $-180^\circ$  crossings should occur when the magnitude of the open loop gain is above 0 dB. The open loop transfer function ( $Y_{ol,i}$ ) corresponding to the closed loop system from

Fig. 6 is given as

$$Y_{ol,i}(s) = G_c(s)G_d(s)Y_{ii}(s), \quad i = 1, 2. \quad (10)$$

The stability of the open loop has a consequent impact on the resonance damping solution of the filter. In addition, for the control system to be stable, the number of encirclements of the critical point  $(-1, 0)$  in the open loop transfer function should not change. The maximum peak criteria is adopted in the following in order to simplify the stability analysis of the filter as indicated in [36]. The maximum peak criteria make use of the sensitivity indicator  $M_S$ , which denotes the amount of resonance (i.e., maximum peaking) in the sensitivity transfer function  $S(s)$  of the control system.  $S(s)$  and  $M_S$  for the current control feedback are defined as [36]

$$\begin{cases} S_i(s) = \frac{1}{1 + Y_{ol,i}(s)}, & i = 1, 2. \\ M_{Si} = \max |S_i(j\omega)| \end{cases} \quad (11)$$

The inverse of the maximum sensitivity gain,  $(M_S)^{-1}$  gives the closest distance between the critical point  $(-1, 0)$  and the open loop transfer function. Therefore, it contains information about both the gain margin and phase margin of the control system. There are generally applicable design guidelines for a control system to be stable and robust, such as  $M_S$  to be lower than 2 (absolute value). Therefore, the lower the value of  $M_S$ , the better the robustness, while for stability and performance of the control system,  $M_S$  should be close to 1 [68]. For  $M_S = 2$ , the closed loop poles are well inside the unit circle and the system is said to be stable (controller damping factor of about 0.7). With this design approach, it becomes easy to guarantee the desired dynamic performance of the system.

### C. Application of Maximum Peak Criteria for Resonance Damping

The critical frequency is an important parameter in deciding the passive damping solution. For a sampling frequency equal with the switching frequency, the critical frequency is 1/6th of the sampling frequency [69]. Then, for the grid current control feedback, no damping is required if the resonance frequency of the filter seen in the control system is higher than the critical frequency [69]. The opposite is true for the converter current control feedback [70].

The maximum sensitivity gains for the two current feedback solutions are illustrated in Fig. 7. Recalling the *LCL* filter design space solutions from Fig. 2, it follows from Fig. 7 that for converter current feedback, adopting no passive damping implies very large ratings of the passive components, which leads to very high cost of the filter. In addition, larger  $L_1$  and lower  $C$  will improve the control stability (it is expected high percentage values of  $L_1$  and lower values of  $C$  and  $L_2$  for a robust filter). For the grid current feedback, it is possible to avoid the use of damping since a large set of filter parameters in the design space fulfill the attenuation requirements. For this case, the stability is mainly improved by decreasing the filter capacitance.

If the operating switching frequency decreases, the available solutions in the design space from Fig. 2 are reduced and the use of damping is mandatory in order to ensure the

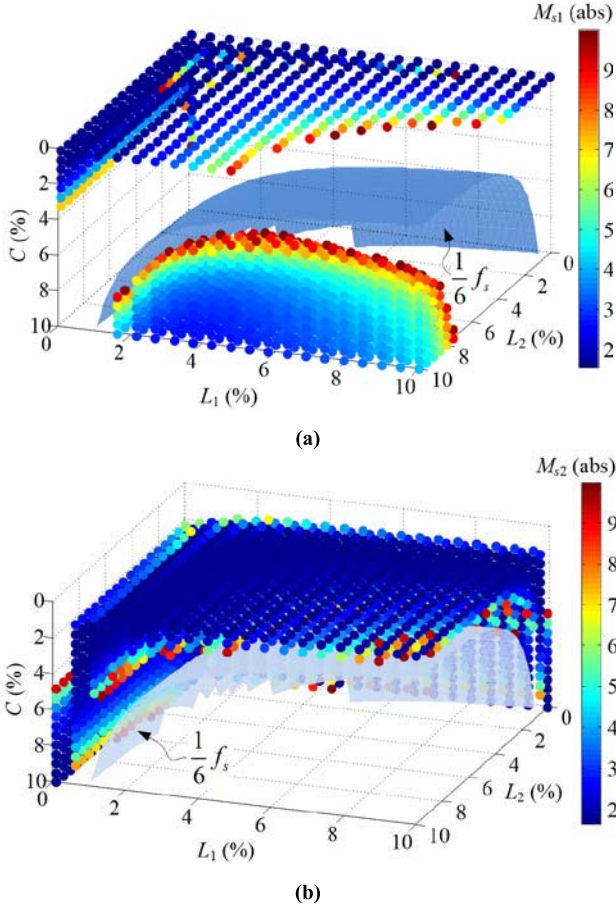


Fig. 7. LCL filter parameter variation as function of the maximum sensitivity ( $M_S$ ) gain, when  $f_s = 10$  kHz. (a) Converter current control. (b) Grid current control.

control stability. In either case, the attenuation of the filter around the resonance frequency of the filter should be carefully investigated. In addition, for good dynamic performance of the control system,  $M_S$  should be chosen no larger than 2. By adding passive damping, the design space from Fig. 2 increases and more solutions are available for the filter designer. Then, in order to reduce the power loss in the damping resistor or to meet some stability or transient performance criteria (such as  $M_S \approx 2$ ), the quality factor of the filter can be decreased and adjusted accordingly until the controller specifications are met.

An illustrative example of the frequency response for the selected passive filters for the converter and grid current feedback control are illustrated in Fig. 8. The passive filters are designed to provide the same attenuation of the dominant harmonics,  $M_S \approx 2$  and an X/R ratio of 2, around the resonance frequency is selected for the inductive components. The attenuation of the filters can be identified from the magnitude diagram illustrated in Fig. 8(b). The sampling delay ( $G_d(s)$ ) of 1.5 sampling periods in the control system is modeled with a second-order Pade approximation [71].

## V. PASSIVE FILTERS EVALUATION

### A. Passive Filter Design Prerequisites

The use of passive damping implies different component ratings depending on the operating conditions, mainly given by

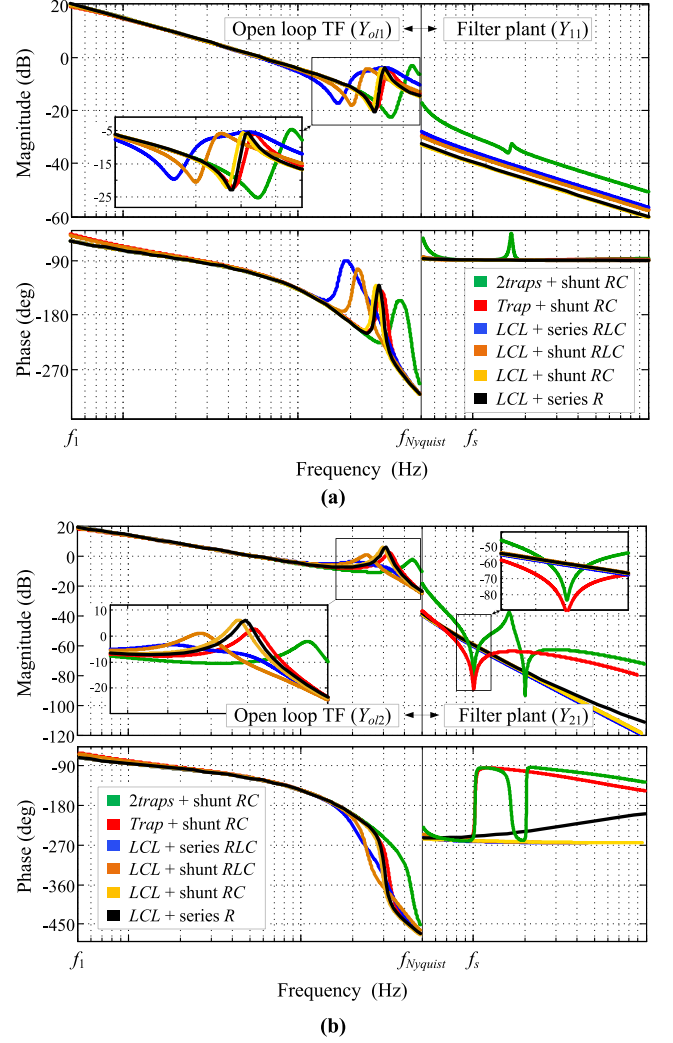


Fig. 8. Frequency response of the passive filters (see Fig. 4) with  $M_S \approx 2$ . (a) Converter current control. (b) Grid current control.

the operating switching frequency, current feedback method, or harmonic attenuation requirement. Therefore, the passive filters are evaluated as a function of the operating switching frequency and current feedback ( $i_1$  for converter and  $i_2$  for the grid current). In addition, two different harmonic standards are considered for the review, one is the BDEW standard, which is more stringent and used for high power applications (switching frequency  $\approx 1$ –5 kHz); the other one is the IEEE 1547, which is more tolerable and can be used for a wide range of applications (switching frequency  $\approx 1$ –15 kHz). All the filters are designed to have the same attenuation of the switching harmonic content, except the trap topologies which are designed in a such a way that harmonics around the multiples of the switching frequency complies with the harmonic regulation limits [37]. The resonance attenuation is selected to be the same for all the passive filters, e.g., the sensitivity gain ( $M_S \approx 2$ ) is the same for all the passive filters.

A conventional asymmetrical SVM with one-third harmonic injection is adopted for minimum current ripple and high dc-link voltage utilization [21]. The dc-link voltage is assumed constant for all switching frequencies. However, a high voltage

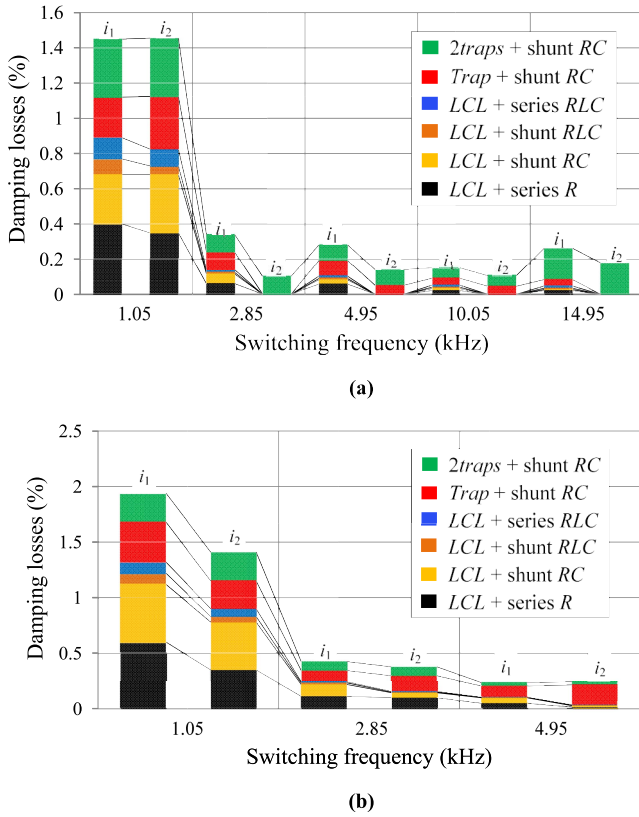


Fig. 9. Damping losses as function of switching frequency for converter ( $i_1$ ) and grid current control ( $i_2$ ) calculated according to [58]. (a) IEEE 1547. (b) BDEW.

drop across the inductors for low switching frequencies can lead to very different results with changing the dc-link voltage [51]. The effect would be less significant for switching frequencies above 2.5 kHz. The VSC is operated with unity power factor. It is expected that the results do not vary significantly with different power factors. The converter side inductor  $L_1$  is the dominant component of the filter since it handles both the fundamental and switching ripple current from the power converter. Therefore, in the following,  $L_1$  is referred to as ripple or PWM inductor.  $L_2$  is referred to as line (sine wave) inductor since it is connected in series with the line impedance. To minimize the size of the filter, the ripple current is chosen variable and dependent on the adopted switching frequency. The same applies for the choice of the filter capacitor  $C$ . In addition, the sampling frequency is adopted equal with the switching frequency.

### B. Passive Damping Losses

The passive filters are designed in such a way to ensure that power losses corresponding to the passive damping circuit are limited to reasonable and practical values. This implies in most of the cases the use of low capacitance values. In Fig. 9, the damping losses are illustrated with different operating switching frequencies of the VSC. The damping losses are averaged for one fundamental period.

For low operating switching frequencies, the damping losses of the series damping resistor is in the same range as the shunt RC damper solution. The key passive damping topologies

are the series and shunt  $RLC$  circuits, which provide close-to-zero damping loss, especially if the switching frequency is higher than 2.85 kHz. For the grid current feedback and IEEE 1547 recommendations, no damping is required for the  $LCL$  filter for frequencies higher than 2.85 kHz. It is not the case for the more stringent attenuation levels as the BDEW recommendations. The damping loss of the  $2traps$  filter is relatively larger than other topologies for the IEEE 1547 recommendations due to the fact that it provides reduced sized inductors, and high ripple current flows into the damping circuit.

### C. Passive Filter Components Ratings

The ratings of the ripple inductance are illustrated in Fig. 10(a). A large difference in the ripple inductance (while keeping the same filter attenuation and dynamic performance) is seen because the ripple in the PWM inductor is chosen variable for different topologies in order to achieve low size of the overall filter.

The size of the line inductance is shown in Fig. 10(b). To guarantee low size of the filter and to ensure the dynamic performance, in case of the converter current feedback, the ripple inductance is chosen higher than the line inductance, while the capacitance is chosen as small as possible to limit the damping loss ( $<0.5\%$ ). For the grid current feedback, the filter inductances are kept around the same, while the capacitance value again is limited. The only exceptions are the series and shunt  $RLC$  damping circuits, which allow increased capacitance size in the filter due to the very low damping loss capability. Hence, low size and cost of these filter solutions can be expected.

The capacitance values are illustrated in Fig. 10(c). No additional damping circuit ratings or trap inductors ratings are given, since these ratings are typically small compared with the main filter components, as it will be shown in Section V-D. In addition, the passive damping loss gives a good indication about the damping resistor ratings and practicability of the damping circuit. The total stored energy in the inductive filter components is shown in Fig. 10(d) in order to evaluate the size of each passive filter. Compared to the  $LCL$  filter, the trap filter can provide 20%~40% reduction in size for switching frequencies above 2.5 kHz. The  $2traps$  configuration can reduce the filter size up to 70% depending on the operating condition. The size of the other passive filters is within  $\pm 20\%$  range. In addition, passive damping does not influence the size of the overall filter by more than 10%.

### D. Passive Damping Performance

Another important evaluation which cannot directly be drawn from the above analysis is that the series and shunt  $RLC$  damping circuits provide more design freedom in the selection of parameters. For example, if more resonance attenuation is required, then it is possible to configure the filters in such a way to obtain low damping loss, which is not the case with the shunt RC damper and the series R damper case. Furthermore, for the BDEW standard it is more difficult to obtain good dynamic performance and to ensure low sensitivity gains.

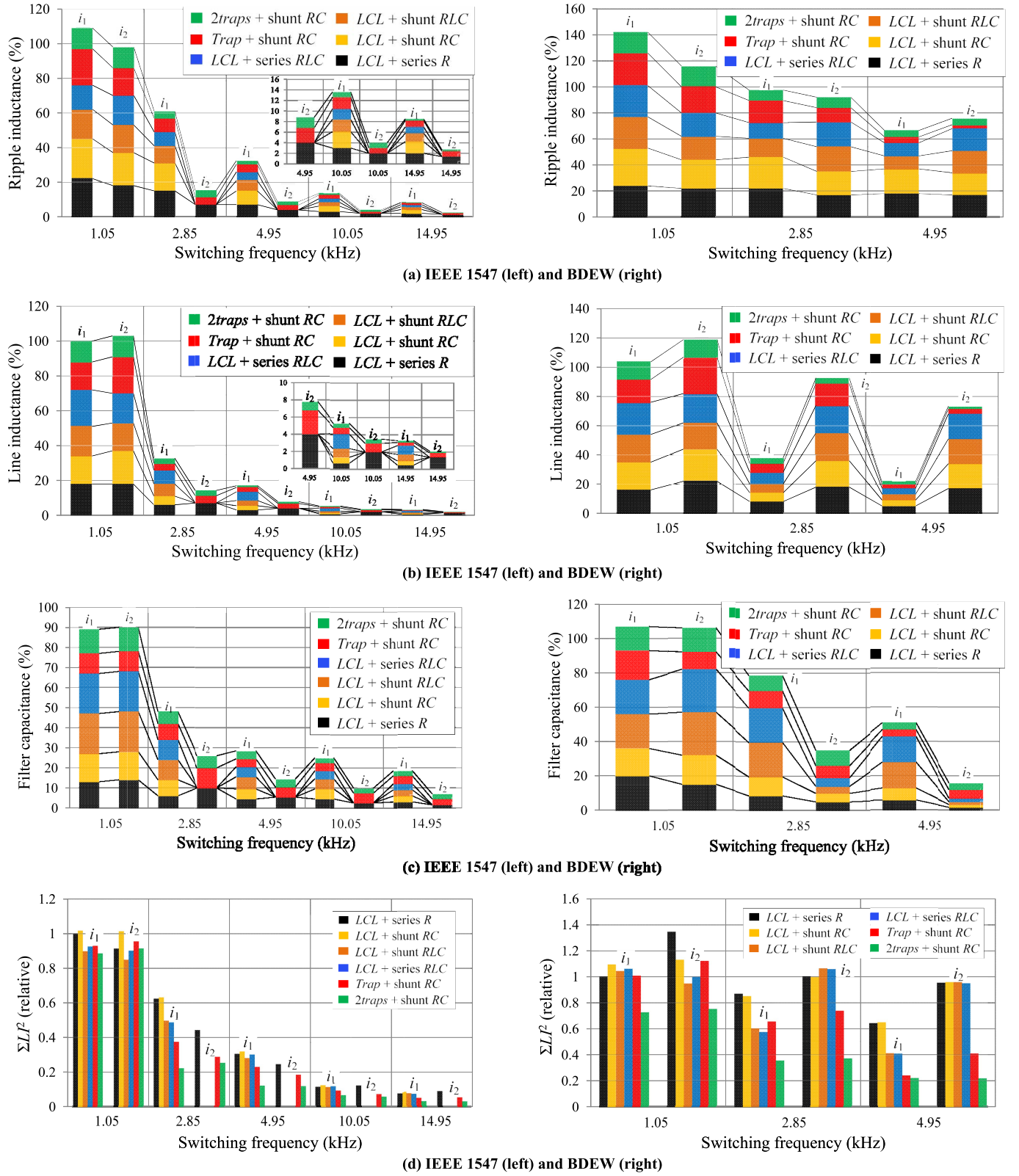


Fig. 10. Filter size evaluation for converter ( $i_1$ ) and grid current control ( $i_2$ ) by (a) ripple inductance, (b) line inductance, (c) total capacitance, and (d) total relative stored energy in inductors (relative to the  $LCL + series R$  damper, converter current control and  $f_s = 1.05$  kHz).

To illustrate the performance of different passive dampers, the power loss in the damping resistor and current controller specifications are shown in Table III by varying the quality

factor of the filters. Since the quality factor of the filters as given in (8) depends on all the filter components, the influence of the filter component tolerance on the specific

TABLE III  
PASSIVE DAMPING EVALUATION AND CURRENT CONTROLLER SPECIFICATIONS

Damping topology	$Q$ [relative]	$Y_{ol,2}$ [dB]		$PM$ [deg]		$GM$ [dB]		$Bw$ [Hz]		$P_d$ [%]	
		$C_{high}$	$C_{low}$	$C_{high}$	$C_{low}$	$C_{high}$	$C_{low}$	$C_{high}$	$C_{low}$	$C_{high}$	$C_{low}$
<i>LCL</i> + Series <i>R</i> $C_{high}=15\%$ ; $C_{low}=1.6\%$ .	$Q = 0.03$	3.65	12.1	89.5	65.3	8.32	5.92	418	1419	0.11	0.0084
	$Q = 0.15$	-3.28	1.4	89.5	65.2	8.33	6.01	258	1322	0.53	0.041
	$Q = 0.3$	-7.2	-3.5	89.5	65.2	8.36	6.17	239	1181	1.05	0.0831
	$Q = 0.45$	-9.2	-6	89.5	65	8.41	6.33	227	1069	1.57	0.123
<i>LCL</i> + Shunt <i>RC</i> $C_{high}=17\%$ $C_{low}=1.65\%$	$0.1 Q_{opt}$	4.7	14.5	89.3	65.2	7.96	5.75	394	1407	0.08	0.0045
	$0.5 Q_{opt}$	0	6.5	89	65.2	8	5.88	378	1391	0.34	0.011
	$Q_{opt}$	-1.2	4.65	89.3	65.2	8.1	6.08	294	1412	0.61	0.016
	$1.5 Q_{opt}$	-0.8	5.4	89.3	65.1	8.2	6.24	265	1444	0.87	0.022
<i>LCL</i> + Series <i>RLC</i> $C_{high}=25\%$ $C_{low}=2\%$	$0.1 Q_{opt}$	3.2	10.9	88.8	64.8	7.11	4.57	344	1268	0.15	0.006
	$0.5 Q_{opt}$	-3.8	0	88.8	64.7	6.97	4.54	298	1180	0.11	0.0053
	$Q_{opt}$	-5.8	-3	88.8	64.7	6.75	4.14	263	1056	0.067	0.003
	$1.5 Q_{opt}$	-5.3	-2.5	88.8	64.7	6.62	3.75	254	992	0.05	0.0024
<i>LCL</i> + Shunt <i>RLC</i> $C_{high}=25\%$ $C_{low}=1.65\%$	$0.1 Q_{opt}$	4.1	12.8	88.9	65.2	7.31	5.75	355	1402	0.08	0.005
	$0.5 Q_{opt}$	-1.9	3.5	88.9	65.2	7.18	5.82	320	1365	0.05	0.004
	$Q_{opt}$	-3.5	1.45	88.9	65	7.1	5.87	294	1358	0.03	0.0025
	$1.5 Q_{opt}$	-2.9	2.3	88.9	65.2	7.8	5.85	288	1404	0.02	0.002
<i>Trap</i> + shunt <i>RC</i> $C_{high}=10\%$ $C_{low}=5\%$	$0.1 Q_{opt}$	3.95	9.2	90	66	9.13	7.87	208	900	0.25	0.52
	$0.5 Q_{opt}$	-1.3	-0.7	90	66	9.23	7.9	206	876	0.28	0.234
	$Q_{opt}$	-2.65	-2.6	90	66	9.23	8	204	843	0.42	0.18
	$1.5 Q_{opt}$	-2.18	-2	90	66	9.23	8.13	201	819	0.58	0.178
<i>2traps</i> + shunt <i>RC</i> $C_{high}=14\%$ $C_{low}=4\%$	$0.1 Q_{opt}$	3.77	10.3	90.17	66.3	9.37	8.56	199	771	0.62	0.035
	$0.5 Q_{opt}$	-1.67	0.68	90.1	66.3	9.37	8.56	198	769	0.27	0.031
	$Q_{opt}$	-3.07	-1.2	90.2	66.3	9.4	5.59	196	763	0.44	0.035
	$1.5 Q_{opt}$	-2.67	-0.5	90.2	66.3	9.44	8.64	194.6	756	0.63	0.052

topology can also be assessed by varying the quality factor. To take into account the influence of the filter capacitance value on the damping loss, two scenarios are considered. One is referred to as a high capacitance scenario ( $C_{high}$ ) and uses the results calculated for 1.05-kHz switching frequency and BDEW specifications. The low capacitance scenario ( $C_{low}$ ) uses the results simulated for 4.95 kHz switching frequency and the same harmonic recommendations.

In Table III is shown how the series *R* and shunt *RC* dampers are limited for the use in high damping situations. The controller bandwidth information can be used to design the range of harmonic compensators, which can suppress the low-order current harmonics that corresponds to voltage background distortion from the utility grid. In addition, the current harmonic order, that can be compensated from the control system, can be increased to the resonance frequency of the filter if a virtual *RC* damping control scheme is adopted in the current controller [72].

## VI. EXPERIMENTAL RESULTS

In order to demonstrate the previous design considerations, the passive filters have been designed for an 11 kW–10 kHz three-phase power converter. The setup used for experimental validation is illustrated in Fig. 11 and comprises a Danfoss FC302 inverter, which is controlled through a dSPACE 1007 platform using P+R current controllers [73]. The dc-link voltage is kept constant from a Yaskawa active rectifier to 700 V. Hence, no dc voltage control loop is used.

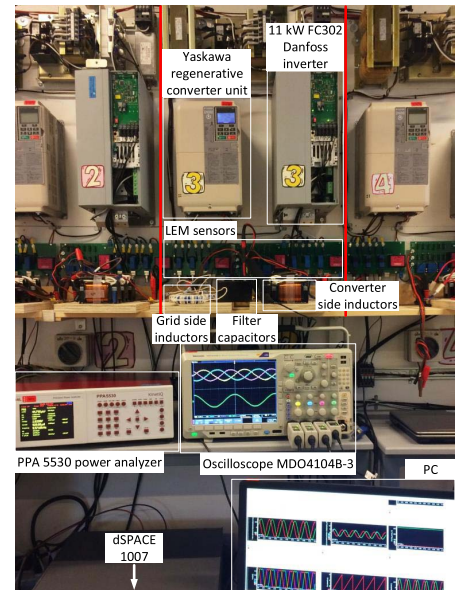


Fig. 11. Experimental hardware setup used for the evaluation of different passive filters.

The experimental setup is connected to a 400 V (line to line voltage), 50 Hz power grid.

The power loss in the resistor and the switching harmonics attenuation are measured using a Newton 4th power analyzer (PPA 5530) and presented in Table IV. In Table V, the ratings of the designed passive filters are illustrated.

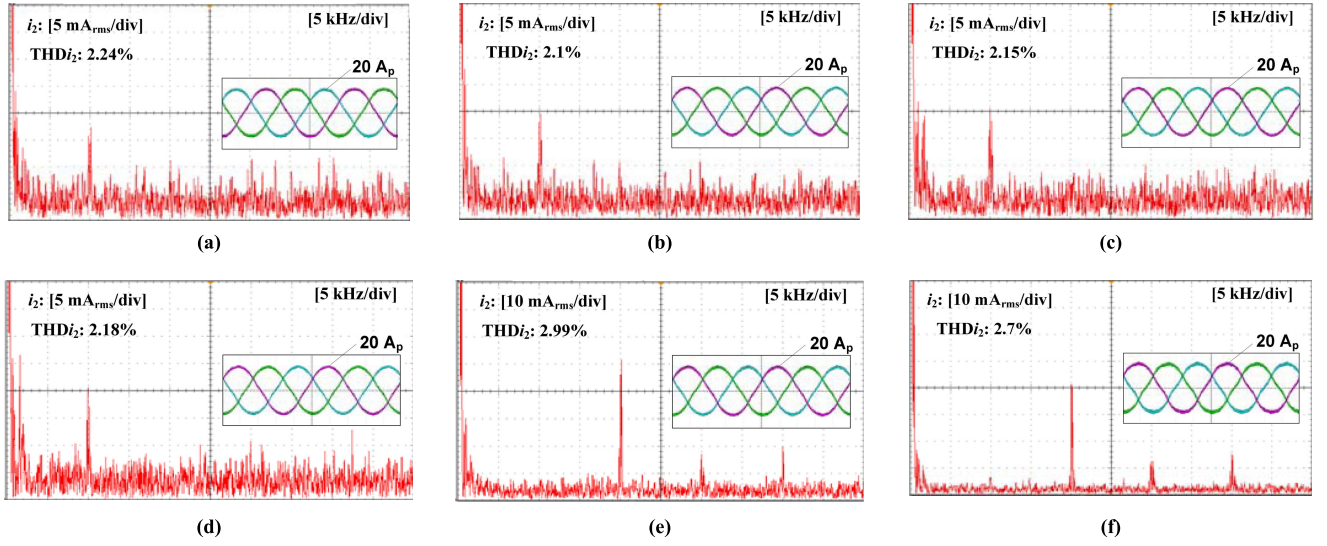


Fig. 12. Harmonic spectrum of the grid current for the selected passive filters topologies. (a) *LCL* + series *R*. (b) *LCL* + shunt *RC*. (c) *LCL* + shunt *RLC*. (d) *LCL* + series *RLC*. (e) Trap + shunt *RC*. (f) 2traps + shunt *RC*.

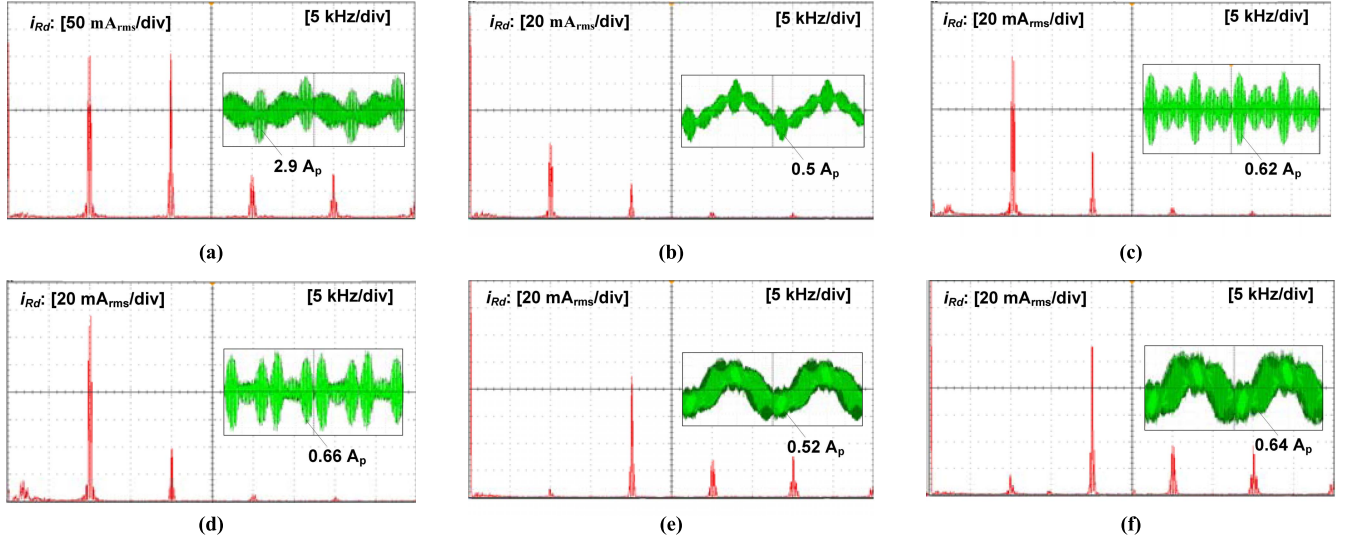


Fig. 13. Harmonic spectrum of the damping current for the selected passive filters topologies. (a) *LCL* + series *R*. (b) *LCL* + shunt *RC*. (c) *LCL* + shunt *RLC*. (d) *LCL* + series *RLC*. (e) Trap + shunt *RC*. (f) 2traps + shunt *RC*.

The grid current waveform and the corresponding harmonic current spectrum are illustrated in Fig. 12. There is no significant difference in the THD of the grid current for the selected passive filters under rated conditions. In rated conditions, the THD is equal to the total demand distortion (TDD).

The power losses in damping resistor can vary by a factor 10, depending on the filter topology. In Fig. 13, the current in the damping resistor is demonstrated at rated conditions. It can be seen that the fundamental current and high-frequency current is very limited for the shunt and series *RLC* dampers according to the aforementioned analysis. For the series *R* and shunt *RC* dampers, the current in the damping resistor is reflected by the value of capacitance and resistors. If the resistance dominates the shunt impedance of the filter, then the damping current will be more sinusoidal and higher damping loss will occur. The power loss mismatch in the damping resistor between the simulated and the measured

TABLE IV  
EVALUATION OF SWITCHING HARMONICS ATTENUATION  
AND POWER LOSS IN DAMPING RESISTOR

Filter Topology	Simulated Power loss (%)	Measured Power loss (%)	Meas. harmonic current, $I_{mf2}$ (%)
<i>LCL</i> + series <i>R</i>	0.197	0.12	0.144%
<i>LCL</i> + shunt <i>RC</i>	0.062	0.045	0.192%
<i>LCL</i> + shunt <i>RLC</i>	0.0455	0.028	0.182%
<i>LCL</i> + series <i>RLC</i>	0.032	0.011	0.165%
Trap + shunt <i>RC</i>	0.0581	0.03	0.048%
2traps + shunt <i>RC</i>	0.0094	0.03	0.042%

values shown in Table IV is related to the damping that exists in the filter and in the grid impedance (more damping exists in the real system than simulated).

TABLE V  
PASSIVE FILTERS COMPONENT RATINGS USED IN EXPERIMENTS (Ap: AMPERE PEAK, Vp: VOLT PEAK, Wp: WATT PEAK)

Filter Topology	Converter Side Inductor		Line Inductor		Filter Capacitors		Damp. Resistor		Damp. Inductor		Damp. Capacitor		Trap Inductors	
	Ap	mH	Ap	mH	Vp	$\mu$ F	Wp	$\Omega$	Ap	mH	Vp	$\mu$ F	Ap	mH
<i>LCL</i> + series <i>R</i>	22.5	1.5	21	1.5	330	4.7	85	5.5	-	-	-	-	-	-
<i>LCL</i> + shunt <i>RC</i>	22.5	1.5	21	1.6	330	2.35	20	41.4	-	-	330	2.15	-	-
<i>LCL</i> + shunt <i>RLC</i>	22.5	1.5	21	1.5	330	2.35	14	20	0.35	3.3	330	2.15	-	-
<i>LCL</i> + series <i>RLC</i>	22.5	1.5	21	1.5	330	4.7	10	6.2	0.75	0.62	8	5.6	-	-
<i>Trap</i> + shunt <i>RC</i>	22.5	1.5	21	0.7	330	2.15	25	20	-	-	330	2.35	3	0.113
<i>2traps</i> + shunt <i>RC</i>	22.5	1.5	21	0.1	330/380	2.15/0.21	8	5.4	-	-	330	2.35	2.8/1.4	0.113/0.3

TABLE VI  
MAIN FEATURES OF PASSIVE FILTERS

Filter Topology	Advantages	Disadvantages	Applications
<i>LCL</i> + series <i>R</i>	1) Simple design and implementation	1) Decreased high frequency attenuation 2) High damping loss for high capacitance and/or high resonance damping	Low power
<i>LCL</i> + shunt <i>RC</i>	1) Lower damping loss 2) Good high frequency attenuation	1) High damping loss for high capacitance and/or high resonance damping	Low power
<i>LCL</i> + shunt <i>RLC</i>	1) Lowest damping loss for high resonance damping 2) Good high frequency attenuation	1) More difficult to implement 2) Requires additional low rated damping inductance (high inductance/low current)	High power
<i>LCL</i> + series <i>RLC</i>	1) Lowest damping loss for high resonance damping 2) Good high frequency attenuation	1) More difficult to implement 2) Requires additional low rated damping inductance (low inductance/high current)	High power
<i>Trap</i> + shunt <i>RC</i>	1) Low filter size and cost	1) Decreased high frequency attenuation 2) More difficult to implement 3) Increased power loss 4) Susceptible to de-tuning	Low and high power
<i>2traps</i> + shunt <i>RC</i>	1) Lowest filter size and cost	1) Decreased high frequency attenuation 2) More difficult to implement 3) Highest power loss due to high ripple content 4) Susceptible to de-tuning	Low and high power

By changing the operating mode of the inverter from rated to light-load or no-load conditions, the TDD of the grid current from Fig. 12 will improve slightly depending on the adopted magnetic materials of the filter inductors. The filter inductance will increase by decreasing the output current due to the permeability decrease of magnetic materials [35], which causes less current ripple in light-load conditions. This effect is less significant for high power applications where the operating switching frequencies are relatively low and the laminated steel is most likely to be adopted for the power inductors (in this case, the permeability dependence with dc bias is relatively constant). The passive damping losses will also decrease slightly with decreasing the output current in applications that uses power inductors designed with powder compounds materials.

## VII. CONCLUSION

In this paper, several passive filters are reviewed in terms of stored energy in the passive components, damping capability

and power loss in the damping circuit. The passive filters are designed to have the same attenuation of the switching harmonic content. The damping circuit is designed to keep about the same resonance attenuation by using the maximum peak criteria (in order to ensure same dynamic performance). Although passive damping itself does not increase the size of the filter significantly, it may increase the power loss in the damping circuit to unacceptable levels, especially in cost/size optimized filters. Therefore, depending on the passive damping solution and the operating conditions, the size and cost of the filter can be much different.

To guarantee low size of the filter and to ensure desired dynamic performance, in the case of the converter current feedback, the ripple inductance is chosen higher than the line inductance, while the capacitance is chosen as minimum as possible in order to limit the damping loss. For the grid current feedback, the filter inductances are kept around the same value while the capacitance value is again limited. The only exceptions are the series and shunt *RLC* damping

circuits, which allow an increased capacitance size in the filter due to close-to-zero damping loss. Such advantages can be obtained from the fact that the series and shunt  $R$ LC damping circuits provides more design freedom in the choice of parameters, because of the additional resonant circuit. For example, if more resonance attenuation is required from the filter, then it is possible to configure the filters in such a way to obtain low damping loss, which is not the case with the series  $R$  and shunt  $RC$  passive dampers. The highest damping loss (around 0.4%) is obtained for low operating switching frequency. With increasing the operating switching frequency, the damping losses hardly exceed 0.1%. A summary of the reviewed passive filters topologies is presented in Table VI.

## REFERENCES

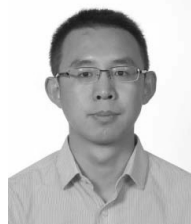
- [1] J. C. Das, "Passive filters—Potentialities and limitations," *IEEE Trans. Ind. Appl.*, vol. 40, no. 1, pp. 232–241, Jan./Feb. 2004.
- [2] D. G. Holmes and T. A. Lipo, *Pulse Width Modulation for Power Converters: Principles and Practice*. New York, NY, USA: Wiley, 2003.
- [3] M. Céspedes and J. Sun, "Mitigation of inverter-grid harmonic resonance by narrow-band damping," *IEEE J. Emerg. Sel. Topics Power Electron.*, vol. 2, no. 4, pp. 1024–1031, Dec. 2014.
- [4] Y. Patel, D. Pixler, and A. Nasiri, "Analysis and design of TRAP and LCL filters for active switching converters," in *Proc. IEEE Int. Symp. Ind. Electron.*, Jul. 2010, pp. 638–643.
- [5] *Power Generation Systems Connected to the Low-Voltage Distribution Network—Technical Minimum Requirements for the Connection to and Parallel Operation With Low-Voltage Distribution Networks*, document VDE-AR-N 4105:2011-08, VDE Verband der Elektrotechnik Elektronik Informationstechnik e.V., 2010.
- [6] *Technical Guideline: Generating Plants Connected to the Medium-Voltage Network*, BDEW, Berlin, Germany, 2008.
- [7] *IEEE Application Guide for IEEE Std 1547, IEEE Standard for Interconnecting Distributed Resources With Electric Power Systems*, IEEE Standard 1547.2-2008, 2009.
- [8] G. Bertotti, "General properties of power losses in soft ferromagnetic materials," *IEEE Trans. Magn.*, vol. 24, no. 1, pp. 621–630, Jan. 1987.
- [9] M. S. Rylko, K. J. Hartnett, J. G. Hayes, and M. G. Egan, "Magnetic material selection for high power high frequency inductors in dc-dc converters," in *Proc. 14th Annu. IEEE Appl. Power Electron. Conf. Expo.*, Feb. 2009, pp. 2043–2049.
- [10] L. Wei and R. A. Lukaszewski, "Optimization of the main inductor in a LCL filter for three phase active rectifier," in *Proc. Conf. Rec. IEEE Ind. Appl. Conf., 42nd IAS Annu. Meeting*, Sep. 2007, pp. 1816–1822.
- [11] R. Teichmann, M. Malinowski, and S. Bernet, "Evaluation of three-level rectifiers for low-voltage utility applications," *IEEE Trans. Ind. Electron.*, vol. 52, no. 2, pp. 471–481, Apr. 2005.
- [12] J. Muhlethaler, M. Schweizer, R. Blattmann, J. W. Kolar, and A. Ecklebe, "Optimal design of LCL harmonic filters for three-phase PFC rectifiers," *IEEE Trans. Power Electron.*, vol. 28, no. 7, pp. 3114–3125, Jul. 2013.
- [13] M. Liserre, F. Blaabjerg, and S. Hansen, "Design and control of an LCL-filter-based three-phase active rectifier," *IEEE Trans. Ind. Appl.*, vol. 41, no. 5, pp. 1281–1291, Sep./Oct. 2005.
- [14] M. A. Abusara and S. M. Sharkh, "Design and control of a grid-connected interleaved inverter," *IEEE Trans. Power Electron.*, vol. 28, no. 2, pp. 748–764, Feb. 2013.
- [15] A. Lesnicar and R. Marquardt, "An innovative modular multilevel converter topology suitable for a wide power range," in *Proc. IEEE Bologna Power Tech Conf.*, vol. 3, Jun. 2003, pp. 272–277.
- [16] A.-S. A. Luiz and B. J. C. Filho, "Analysis of passive filters for high power three-level rectifiers," in *Proc. 34th Annu. Conf. IEEE Ind. Electron.*, Nov. 2008, pp. 3207–3212.
- [17] K. Jalili and S. Bernet, "Design of LCL filters of active-front-end two-level voltage-source converters," *IEEE Trans. Ind. Electron.*, vol. 56, no. 5, pp. 1674–1689, May 2009.
- [18] A. M. Hava, T. A. Lipo, and W. L. Erdman, "Utility interface issues for line connected PWM voltage source converters: A comparative study," in *Proc. IEEE Appl. Power Electron. Conf. Expo.*, Mar. 1995, pp. 125–132.
- [19] J. Sun, "Impedance-based stability criterion for grid-connected inverters," *IEEE Trans. Power Electron.*, vol. 26, no. 11, pp. 3075–3078, Nov. 2011.
- [20] M. Céspedes and J. Sun, "Impedance modeling and analysis of grid-connected voltage-source converters," *IEEE Trans. Power Electron.*, vol. 29, no. 3, pp. 1254–1261, Mar. 2014.
- [21] J. C. Das, *Power System Harmonics and Passive Filter Designs*. Piscataway, NJ, USA: Wiley, 2015.
- [22] M. Liserre, A. Dell'Aquila, and F. Blaabjerg, "Genetic algorithm-based design of the active damping for an LCL-filter three-phase active rectifier," *IEEE Trans. Power Electron.*, vol. 19, no. 1, pp. 76–86, Jan. 2004.
- [23] G. Zeng, T. W. Rasmussen, and R. Teodorescu, "A novel optimized LCL-filter designing method for grid connected converter," in *Proc. 2nd IEEE Int. Symp. Power Electron. Distrib. Generat. Syst.*, vol. 2, Jun. 2010, pp. 802–805.
- [24] J. Verveckken, J. F. Silva, and J. Driesen, "Optimal analytic LCL filter design for grid-connected voltage-source converter," in *Proc. EuroCon*, Jul. 2013, pp. 823–830.
- [25] L. Shen, G. Asher, P. Wheeler, and S. Bozhko, "Optimal LCL filter design for 3-phase space vector PWM rectifiers on variable frequency aircraft power system," in *Proc. 15th Eur. Conf. Power Electron. Appl. (EPE)*, Sep. 2013, pp. 1–8.
- [26] X. Wang, F. Blaabjerg, and P. C. Loh, "Grid-current-feedback active damping for LCL resonance in grid-connected voltage-source converters," *IEEE Trans. Power Electron.*, vol. 31, no. 1, pp. 213–223, Jan. 2016.
- [27] J. Arrillaga and N. R. Watson, *Power System Harmonics*. Chichester, U.K.: Wiley, 2003.
- [28] J. Shen, S. Schroder, H. Stagge, and R. W. De Doncker, "Impact of modulation schemes on the power capability of high-power converters with low pulse ratios," *IEEE Trans. Power Electron.*, vol. 29, no. 11, pp. 5696–5705, Nov. 2014.
- [29] T. C. Y. Wang, Z. Ye, G. Sinha, and X. Yuan, "Output filter design for a grid-interconnected three-phase inverter," in *Proc. IEEE 34th Annu. Power Electron. Specialist Conf. (PESC)*, vol. 2, Jun. 2003, pp. 779–784.
- [30] K. H. Ahmed, S. J. Finney, and B. W. Williams, "Passive filter design for three-phase inverter interfacing in distributed generation," in *Proc. Compat. Power Electron.*, May/Jun. 2007, pp. 1–9.
- [31] R. Peña-Alzola, M. Liserre, F. Blaabjerg, R. Sebastián, J. Dannehl, and F. W. Fuchs, "Analysis of the passive damping losses in LCL-filter-based grid converters," *IEEE Trans. Power Electron.*, vol. 28, no. 6, pp. 2642–2646, Jun. 2013.
- [32] A. A. Rockhill, M. Liserre, R. Teodorescu, and P. Rodriguez, "Grid-filter design for a multimewatt medium-voltage voltage-source inverter," *IEEE Trans. Ind. Electron.*, vol. 58, no. 4, pp. 1205–1217, Apr. 2011.
- [33] W. Wu *et al.*, "A robust passive damping method for LLCL-filter-based grid-tied inverters to minimize the effect of grid harmonic voltages," *IEEE Trans. Power Electron.*, vol. 29, no. 7, pp. 3279–3289, Jul. 2014.
- [34] R. Beres, X. Wang, F. Blaabjerg, C. L. Bak, and M. Liserre, "Comparative analysis of the selective resonant LCL and LCL plus trap filters," in *Proc. Int. Conf. Optim. Elect. Electron. Equip. (OPTIM)*, May 2014, pp. 740–747.
- [35] R. N. Beres, X. Wang, F. Blaabjerg, M. Liserre, and C. L. Bak, "Optimal design of high-order passive-damped filters for grid-connected applications," *IEEE Trans. Power Electron.*, vol. 31, no. 4, pp. 2083–2098, Mar. 2016.
- [36] S. Vesti, T. Suntio, J. A. Oliver, R. Prieto, and J. A. Cobos, "Impedance-based stability and transient-performance assessment applying maximum peak criteria," *IEEE Trans. Power Electron.*, vol. 28, no. 5, pp. 2099–2104, May 2013.
- [37] W. Wu, Y. He, and F. Blaabjerg, "An LLCL power filter for single-phase grid-tied inverter," *IEEE Trans. Power Electron.*, vol. 27, no. 2, pp. 782–789, Feb. 2012.
- [38] Y. Lang, D. Xu, S. R. Hadianamrei, and H. Ma, "A novel design method of LCL type utility interface for three-phase voltage source rectifier," in *Proc. IEEE 36th Power Electron. Specialists Conf.*, Jun. 2005, pp. 313–317.
- [39] S. Jung, Y. Bae, S. Choi, and H. Kim, "A low cost utility interactive inverter for residential fuel cell generation," *IEEE Trans. Power Electron.*, vol. 22, no. 6, pp. 2293–2298, Nov. 2007.
- [40] S. V. Araujo, A. Engler, B. Sahan, and F. L. M. Antunes, "LCL filter design for grid-connected NPC inverters in offshore wind turbines," in *Proc. 7th Int. Conf. Power Electron.*, Oct. 2007, pp. 1133–1138.
- [41] Y. Tang, P. C. Loh, P. Wang, F. H. Choo, and K. K. Tan, "Improved one-cycle-control scheme for three-phase active rectifiers with input inductor-capacitor-inductor filters," *IET Power Electron.*, vol. 4, no. 5, pp. 603–614, May 2011.

- [42] A. Reznik, M. G. Simoes, A. Al-Durra, and S. M. Mueen, "LCL filter design and performance analysis for grid-interconnected systems," *IEEE Trans. Ind. Appl.*, vol. 50, no. 2, pp. 1225–1232, Mar./Apr. 2014.
- [43] Y. Jiao and F. C. Lee, "LCL filter design and inductor current ripple analysis for a three-level NPC grid interface converter," *IEEE Trans. Power Electron.*, vol. 30, no. 9, pp. 4659–4668, Sep. 2015.
- [44] R. W. Erickson and D. Maksimović, *Fundamentals of Power Electronics*. Boston, MA, USA: Springer, 2001.
- [45] M. Liserre, F. Blaabjerg, and A. Dell'Aquila, "Step-by-step design procedure for a grid-connected three-phase PWM voltage source converter," *Int. J. Electron.*, vol. 91, no. 8, pp. 445–460, Aug. 2004.
- [46] B. Bolsens, K. De Brabandere, J. Van den Keybus, J. Driesen, and R. Belmans, "Model-based generation of low distortion currents in grid-coupled PWM-inverters using an LCL output filter," *IEEE Trans. Power Electron.*, vol. 21, no. 4, pp. 1032–1040, Jul. 2006.
- [47] M. Prodanovic and T. C. Green, "Control and filter design of three-phase inverters for high power quality grid connection," *IEEE Trans. Power Electron.*, vol. 18, no. 1, pp. 373–380, Jan. 2003.
- [48] R. Teodorescu, F. Blaabjerg, U. Borup, and M. Liserre, "A new control structure for grid-connected LCL PV inverters with zero steady-state error and selective harmonic compensation," in *Proc. 19th Annu. IEEE Appl. Power Electron. Conf. Expo. (APEC)*, vol. 1, 2004, pp. 580–586.
- [49] X. Zheng, L. Xiao, Y. Lei, and Z. Wang, "Optimisation of LCL filter based on closed-loop total harmonic distortion calculation model of the grid-connected inverter," *IET Power Electron.*, vol. 8, no. 6, pp. 860–868, 2015.
- [50] R. Meyer and A. Mertens, "Design and optimization of LCL filters for grid-connected converters," in *Proc. 15th Int. Power Electron. Motion Control Conf. (EPE/PEMC)*, Sep. 2012, pp. LS7a.1-1–LS7a.1-6.
- [51] K.-B. Park, F. Kieferndorf, U. Drogenik, S. Pettersson, and F. Canales, "Weight minimization of LCL filters for high power converters," in *Proc. 9th Int. Conf. Power Electron. ECCE Asia (ICPE-ECCE Asia)*, Jun. 2015, pp. 142–149.
- [52] T. Shimizu and S. Iyasu, "A practical iron loss calculation for AC filter inductors used in PWM inverters," *IEEE Trans. Ind. Electron.*, vol. 56, no. 7, pp. 2600–2609, Jul. 2009.
- [53] L. Wei, Y. Patel, and C. S. N. Murthy, "Evaluation of LCL filter inductor and active front end rectifier losses under different PWM method," in *Proc. IEEE Energy Convers. Congr. Expo.*, Sep. 2013, pp. 3019–3026.
- [54] H. Matsumori, K. Takano, H. Ishii, and T. Shimizu, "Evaluation of iron loss of ac filter inductor used in three-phase PWM inverters based on an iron loss analyzer," *IEEE Trans. Power Electron.*, vol. 31, no. 4, pp. 3080–3095, Apr. 2016.
- [55] R. C. Dugan, M. F. McGranaghan, S. Santoso, and H. W. Beaty, *Electrical Power Systems Quality*. New York, NY, USA: McGraw-Hill, 2002.
- [56] R. D. Middlebrook, "Design techniques for preventing input-filter oscillations in switched-mode regulators," in *Proc. 5th Nat. Solid-State Power Convers. Conf.*, May 1978, pp. A3.1–A3.16.
- [57] T. K. Phelps and W. S. Tate, "Optimizing passive input filter design," in *Proc. 6th Nat. Solid-State Power Convers. Conf.*, May 1979, pp. G1.1–G1.10.
- [58] P. Channegowda and V. John, "Filter optimization for grid interactive voltage source inverters," *IEEE Trans. Ind. Electron.*, vol. 57, no. 12, pp. 4106–4114, Dec. 2010.
- [59] A. M. Cantarellas, E. Rakhshani, D. Remon, and P. Rodriguez, "Design of the LCL+trap filter for the two-level VSC installed in a large-scale wave power plant," in *Proc. IEEE Energy Convers. Congr. Expo.*, Sep. 2013, pp. 707–712.
- [60] J. Xu, J. Yang, J. Ye, Z. Zhang, and A. Shen, "An LTCL filter for three-phase grid-connected converters," *IEEE Trans. Power Electron.*, vol. 29, no. 8, pp. 4322–4338, Aug. 2014.
- [61] F. Li, X. Zhang, H. Zhu, H. Li, and C. Yu, "An LCL-LC filter for grid-connected converter: Topology, parameter, and analysis," *IEEE Trans. Power Electron.*, vol. 30, no. 9, pp. 5067–5077, Sep. 2015.
- [62] G. Gohil, L. Bede, R. Teodorescu, T. Kerekes, and F. Blaabjerg, "Line filter design of parallel interleaved VSCs for high-power wind energy conversion systems," *IEEE Trans. Power Electron.*, vol. 30, no. 12, pp. 6775–6790, Dec. 2015.
- [63] W. Wu, Y. He, T. Tang, and F. Blaabjerg, "A new design method for the passive damped LCL and LLCL filter-based single-phase grid-tied inverter," *IEEE Trans. Ind. Electron.*, vol. 60, no. 10, pp. 4339–4350, Oct. 2013.
- [64] J. M. Bloemink and T. C. Green, "Reducing passive filter sizes with tuned traps for distribution level power electronics," in *Proc. 14th Eur. Conf. Power Electron. Appl. (EPE)*, Aug./Sep. 2011, pp. 1–9.
- [65] A. M. Cantarellas, E. Rakhshani, D. Remon, and P. Rodriguez, "Design of passive trap-LCL filters for two-level grid connected converters," in *Proc. 15th Eur. Conf. Power Electron. Appl. (EPE)*, Sep. 2013, pp. 1–9.
- [66] Y. Miwa and T. Shimizu, "Loss comparison of core materials used for the inductor of a buck-chopper circuit," in *Proc. IEEE Energy Convers. Congr. Expo. (ECCE)*, Sep. 2015, pp. 5279–5286.
- [67] M. Liserre, A. Dell'Aquila, and F. Blaabjerg, "Stability improvements of an LCL-filter based three-phase active rectifier," in *Proc. IEEE 33rd Annu. IEEE Power Electron. Specialists Conf.*, vol. 3, 2002, pp. 1195–1201.
- [68] S. Skogestad and I. Postlethwaite, *Multivariable Feedback Control: Analysis and Design*, 2nd ed. New York, NY, USA: Wiley, 2005.
- [69] S. G. Parker, B. P. McGrath, and D. G. Holmes, "Regions of active damping control for LCL filters," *IEEE Trans. Ind. Appl.*, vol. 50, no. 1, pp. 424–432, Jan./Feb. 2014.
- [70] C. Zou, B. Liu, S. Duan, and R. Li, "Influence of delay on system stability and delay optimization of grid-connected inverters with LCL filter," *IEEE Trans. Ind. Informat.*, vol. 10, no. 3, pp. 1775–1784, Aug. 2014.
- [71] R. Peña-Alzola, M. Liserre, F. Blaabjerg, R. Sebastián, J. Dannehl, and F. W. Fuchs, "Systematic design of the lead-lag network method for active damping in LCL-filter based three phase converters," *IEEE Trans. Ind. Informat.*, vol. 10, no. 1, pp. 43–52, Feb. 2014.
- [72] X. Wang, F. Blaabjerg, and P. C. Loh, "Virtual RC damping of LCL-filtered voltage source converters with extended selective harmonic compensation," *IEEE Trans. Power Electron.*, vol. 30, no. 9, pp. 4726–4737, Sep. 2015.
- [73] R. Teodorescu, F. Blaabjerg, M. Liserre, and P. C. Loh, "Proportional-resonant controllers and filters for grid-connected voltage-source converters," *IEEE Proc.-Electr. Power Appl.*, vol. 153, no. 5, pp. 750–762, Sep. 2006.



**Remus Narcis Beres** (S'13) received the M.Sc. degree in electrical engineering from the Transilvania University of Brasov, Brasov, Romania, in 2012, and the M.Sc. degree in wind power systems from Aalborg University, Aalborg, Denmark, in 2013, where he is currently pursuing the Ph.D. degree in power filters.

He was with Distribution Network Operator, Electrica Distribution South Transylvania, Brasov, from 2010 to 2011. He was a Visiting Scholar with Tokyo Metropolitan University, Hachioji, Japan, in 2015. His current research interests include power electronics for distributed generation, power quality, and passive components characterization.



**Xiongfei Wang** (S'10–M'13) received the B.S. degree in electrical engineering from Yanshan University, Qinhuangdao, China, in 2006, the M.S. degree in electrical engineering from the Harbin Institute of Technology, Harbin, China, in 2008, and the Ph.D. degree from Aalborg University, Aalborg, Denmark, in 2013.

He has been with Aalborg University since 2009, where he is currently an Assistant Professor with the Department of Energy Technology. His current research interests include modeling and control of grid-connected converters, harmonics analysis and control, passive and active filters, and stability of power electronic-based power systems.

Dr. Wang received the IEEE TRANSACTIONS ON POWER ELECTRONICS Prize Paper Award in 2014. He is an Associate Editor of the IEEE TRANSACTIONS ON INDUSTRY APPLICATIONS, and serves as the Guest Associate Editor of the IEEE JOURNAL OF EMERGING AND SELECTED TOPICS IN POWER ELECTRONICS of the Special Issue on Harmonic Stability and Mitigation in Power Electronics-Based Power Systems and the Special Issue on Distributed Generation.



**Marco Liserre** (S'00–M'02–SM'07–F'13) received the M.Sc. and Ph.D. degrees in electrical engineering from the Polytechnic University of Bari, Bari, Italy, in 1998 and 2002, respectively.

He has been an Associate Professor with the Polytechnic University of Bari and a Professor of Reliable Power Electronics with Aalborg University, Aalborg, Denmark. He is currently a Full Professor and the Chair of Power Electronics with the University of Kiel, Kiel, Germany. He has

published over 200 technical papers (more than 60 of them in international peer-reviewed journals), four chapters of a book, and a book entitled *Grid Converters for Photovoltaic and Wind Power Systems* (IEEE-Wiley), which is translated into Chinese. These works have received more than 12 000 citations.

Dr. Liserre is a Senior Member of the Industrial Electronics Society (IES) AdCom. He is a member of the Industrial Applications Society, the Power Electronics Society, the Power & Energy Society, and the Institution of Engineers. He received the IES 2009 Early Career Award, the IES 2011 Anthony J. Hornfeck Service Award, the 2014 Dr. Bimal Bose Energy Systems Award, the 2011 *Industrial Electronics Magazine* Best Paper Award, and the 2012 Third Prize Paper Award by the Industrial Power Converter Committee at the European Congress of Chemical Engineering. He has received an ERC Consolidator Grant for an overall budget of 2€ million for the project The Highly Efficient and Reliable Smart Transformer, a new Heart for the Electric Distribution System. He was listed in ISI Thomson report The World's Most Influential Scientific Minds in 2014. He is an Associate Editor of the IEEE TRANSACTIONS ON INDUSTRIAL ELECTRONICS, the *IEEE Industrial Electronics Magazine*, and the IEEE TRANSACTIONS ON INDUSTRIAL INFORMATICS, and the Coeditor-in-Chief of the IEEE TRANSACTIONS ON POWER ELECTRONICS and the IEEE JOURNAL OF EMERGING AND SELECTED TOPICS IN POWER ELECTRONICS. He has been the Founder and Editor-in-Chief of the IEEE INDUSTRIAL ELECTRONICS MAGAZINE, the Founder and Chairman of the Technical Committee on Renewable Energy Systems, and the IES Vice President responsible for the publications. He was the Co-Chairman of the International Symposium on Industrial Electronics in 2010.



**Frede Blaabjerg** (S'86–M'88–SM'97–F'03) was with ABB-Scandia, Randers, Denmark, from 1987 to 1988. From 1988 to 1992, he was a Ph.D. Student with Aalborg University, Aalborg, Denmark. He became an Assistant Professor in 1992, an Associate Professor in 1996, and a Full Professor of Power Electronics and Drives in 1998. His current research interests include power electronics and its applications, such as in wind turbines, PV systems, reliability, harmonics, and adjustable speed drives.

Dr. Blaabjerg has received 15 IEEE Prize Paper Awards, the IEEE Power Electronics Society (PELS) Distinguished Service Award in 2009, the EPE-PEMC Council Award in 2010, the IEEE William E. Newell Power Electronics Award in 2014, and the Villum Kann Rasmussen Research Award in 2014. He was the Editor-in-Chief of the IEEE TRANSACTIONS ON POWER ELECTRONICS from 2006 to 2012. He was a Distinguished Lecturer of the IEEE PELS from 2005 to 2007, and the IEEE Industry Applications Society from 2010 to 2011.



**Claus Leth Bak** (SM'99) was born in Århus, Denmark, in 1965. He received the B.Sc. (Hons.) and M.Sc. degrees in electrical power engineering from the Department of Energy Technology, Aalborg University (AAU), Aalborg, Denmark, in 1992 and 1994, respectively.

He was a Professional Engineer in Electric Power Transmission and Substations with specializations in Power System Protection with NV Net Transmission Company, Vodskov, Denmark. In 1999, he was an Assistant Professor with the Department of Energy Technology, AAU, where he is currently a Professor. He has supervised 15 Ph.D. students and over 50 M.Sc. theses. He has authored or co-authored around 120 publications. His current research interests include corona phenomena on overhead lines, power system modeling and transient simulations, underground cable transmission, power system harmonics, power system protection, and HVdc-voltage source converter offshore transmission networks.

Prof. Bak is a member of Cigré C4.502, the Cigré SC C4 Study Committee, and the Danish Cigré National Committee.